
Article:
Brambila, C., Nutter, J., Molinari, M. et al. (4 more authors) (2022) Void space and secondary oriented attachment mechanisms in cerium oxide nanorods. Journal of Nanoparticle Research, 24 (11). 227. ISSN 1388-0764

https://doi.org/10.1007/s11051-022-05598-x

J Nanopart Res (2022) 24:227
https://doi.org/10.1007/s11051-022-05598-x

RESEARCH PAPER

Void space and secondary oriented attachment mechanisms in cerium oxide nanorods

C. Brambila · J. Nutter · M. Molinari · D. C. Sayle · T. Sakthivel · S. Seal · G. Möbus

Received: 29 April 2022 / Accepted: 13 October 2022 / Published online: 3 November 2022

Abstract Two new processes occurring during nanorod annealing of ceria are disclosed, both belonging to the wider "oriented attachment" (OA) scheme of crystal growth, which commonly drives nanoparticles growing into nanorods. The first new process is an inversion of the standard OA, where the usual solid particles are replaced by well-facetted shape-equilibrated voids inside larger single crystals. The internal facetted voids are then found to aggregate during dry heat treatment into rod-shaped elongated voids growing eventually towards nanotubes. For the case of CeO_2, a perfect equivalence is found between positive OA, involving cuboctahedral {111}/{100} nanoparticles turning into {110}/{100} nanorods, and negative or void space OA, where cuboctahedral voids turn into negative tubular rods of same indexing. The second OA process ("secondary OA") concerns aggregation of small nanorod segments into larger, double, or quadruple sized nanorods, with perfection of alignment and bonding exceeding simple van der Waals forces. Eventually, the new rods merge into single crystal grain boundary–free larger rods, but with an external shape, including double-ended rods, indicating their origin from several rods. Both processes are found on identical samples and occur in parallel.

Keywords CeO_2 · Cerium oxide · Nanorods · Oriented attachment · Mesopores · Electron microscopy · Catalyst

C. Brambila · J. Nutter · G. Möbus (✉)
Department of Materials Science and Engineering, University of Sheffield, Sheffield S1 3JD, UK
e-mail: g.moebus@sheffield.ac.uk

J. Nutter
The Henry Royce Institute, Sir Robert Hadfield Building, Sheffield S1 3JD, UK

M. Molinari
Department of Chemistry, University of Huddersfield, Huddersfield HD1 3DH, UK

D. C. Sayle
School of Physical Sciences, University of Kent, Canterbury CT2 7NZ, UK

T. Sakthivel · S. Seal
Advanced Materials Processing and Analysis Center, Nanoscience and Technology Center (NSTC), Mechanical, Materials and Aerospace Engineering (MMAE), College of Medicine, Biionix Cluster, University of Central Florida, Orlando, FL 32816, USA

Introduction

While ceria nanoparticles (CNPs) are amongst the most widely studied and applied functional oxide nanoparticles [1–3], there has been an increasing tendency over the last few decades to increase their functional activity. Often, CNPs are found in (equilibrium) octahedral shape, and the main {111} facets are less suitable for applications involving oxygen storage and extraction, such as in catalysis as revealed

in multiple studies on ceria surface chemistry [4–6]. The main improvement is through the promotion of higher activity facets {110} and {100}, which is achieved through either cube-shaped particles [7–10] or nanorods (CNR) [1, 11–14]. CNRs follow a similar synthesis as CNPs using hydrothermal reactors, but with a different setting for parameters (T, p, t) for temperature, pressure, and time. Phase diagrams have been proposed for promoting rods or cubes compared to octahedral particles, and generally high-quality single crystalline nanorods can be grown in large quantities [15–18].

Another branch of research has concentrated on the defect chemistry of CNRs. While generally detrimental for mechanical applications, defects may be helpful in promoting highly active surface sites and allow more flexibility in tuning catalytic activities. Vacancy and cluster defects in ceria have been modelled [19] and imaged by electron microscopy [20]. High-resolution TEM micrographs of hydrothermally grown CNRs often show low crystalline lattice quality indicating a high point defect concentration distributed homogeneously over the rod [21, 22]. However, after post-synthesis secondary dry heat treatment (e.g. 600–900 °C), extended pores or voids, condensed from aggregated vacancies, form, either in spherical shape [7] or polyhedral [22, 23], or as through-holes [24]. These voids have been likened to "missing" or "negative" CNPs, comprising of e.g. cube-octahedra of about 2–5 nm diameter inside CNRs of 10–30 nm width. The main characteristic is that almost all these voids locate within the CNRs and stay clear of the surface by at least 2 nm. In related materials, e.g. TiO_2 and UO_2, such meso-voids have also been described [25, 26].

The possibility of nano-objects growing out of pre-existing particles, rather than growing atom-by-atom from a single nucleus, has been originally proposed for oxides and referred to as oriented attachment (OA) [27, 28]. OA is now well-established [29, 30], including for ceria [12, 31]. A major achievement is the explanation of the anisotropic growth of nanorods from materials with cubic unit cells [32, 33].

In our latest study about voids in ceria nanorods [23], 3D void morphology was established by electron tomography for most voids having an isotropic shape (cuboctahedral). A small number of voids had been found which appeared as having an elongated shape, which therefore triggered the research focus of the present manuscript: This topic is closely related to the occurrence of ceria nanotubes (CNTs) [34–37], as the tubes may be seen as the ultimate result if all voids in a CNR are merged, symmetrized, and centred on the rod axis. The key subject of the present study is the void formation mechanisms and the proposed relationship to an "oriented attachment" growth of void space.

Simultaneous to the finding of 1D voids, our same heat-treated samples also show CNRs that appear to have originated from multiple individual building blocks. These building blocks are however not the original octahedral NPs as in primary oriented attachment, but smaller pre-existing CNRs. The idea of bundle formation of multiple nanorods has been presented before, e.g. for the case of ceria by Stelmachowski et al. [38], and for other materials such as hydroxyapatite [39]. However, in such previous research neighbouring rods are still rather loosely connected, not perfectly parallel, and certainly not exhibiting atomic bonds at the rod-to-rod interfaces. Our aim here is to elucidate atomically sharp rod-bonding interfaces, using HRTEM imaging, to progress over those earlier studies. At the same time, we also aim to discuss the void formation and rod attachment as simultaneous events, all observed at lattice resolution, and all under the umbrella concept of oriented attachment.

Experimental methods

The hydrothermal process route of our materials is described in detail by Sakthivel et al. [15, 22]. For short, a $Ce(NO_3)_3{\cdot}6H_2O$ precursor is dissolved in deionised water and mixed under stirring with diluted NaOH as the precipitation agent. The resulting slurry is heated in an autoclave to temperatures of 120 °C. Reaction parameters of time, concentration, and temperature have been shifted to maximise the percentage of rod-shaped nanoparticles over octahedral nanoparticles. After cooling and drying, a secondary heat treatment was performed by air heating in a furnace to either 800 °C or 950 °C. This annealing was then followed by TEM specimen preparation putting small samples of powder suspensions in deionised water onto holey carbon film. Where annotated in the figures, a modified procedure was used to reverse TEM film preparation and heating. Here, powder was

suspended onto Si/Si_3N_4 TEM carrier films, which after drying were heated in the same air furnace to the same temperatures.

The transmission electron microscope used for the present study is a field-emission TEM JEOL JEM-F200 with a Gatan OneView CCD camera, operated at 200 kV.

Results

Nanorod morphology

In our previous work, pores or voids of "missing particle" shape showing perfect cuboctahedral morphology have been introduced and characterised by aberration-corrected TEM [20] and electron tomography [23], along with complementary molecular modelling to elucidate the energetics of rod surface and void surface formation. Here, we explore hydrothermally produced nanorods of CeO_2 subjected to secondary heat treatment in a dry furnace at 800 °C and 950 °C, with the two temperatures being chosen to be either below or just above the sintering onset threshold. The sintering threshold is defined here by the onset of external shape changes of CNPs and CNRs, e.g. rounding of corners and rod-ends.

Figure 1 shows side by side the microstructure and morphology of a typical sample before and after heat treatment to 800 °C.

At first, we find that after heating internal voids of well-facetted shape are robust and persist against annihilation or diffusion towards the surface of the rod. Also, all rods retain their shape and sharpness of corners, indicating that there is not yet any Ostwald ripening between neighbouring rods. However, we find that the distribution of the shape of voids now also includes more elongated shapes beyond the simple isotropic morphologies (e.g. cuboctahedra). Indeed, aspect ratios larger than 2:1 are here far more prominent compared to our earlier work [22, 23]. Before interpreting the elongated voids, the external rod shape needs to be reminded. We work on a mix of two types of rods, each showing a non-regular hexagon cross-section.

- Type 1 is enclosed by {100}/{110} facets along a < 110 > axis.
- Type 2 is enclosed by {111}/{110} facets along a < 211 > rod axis.

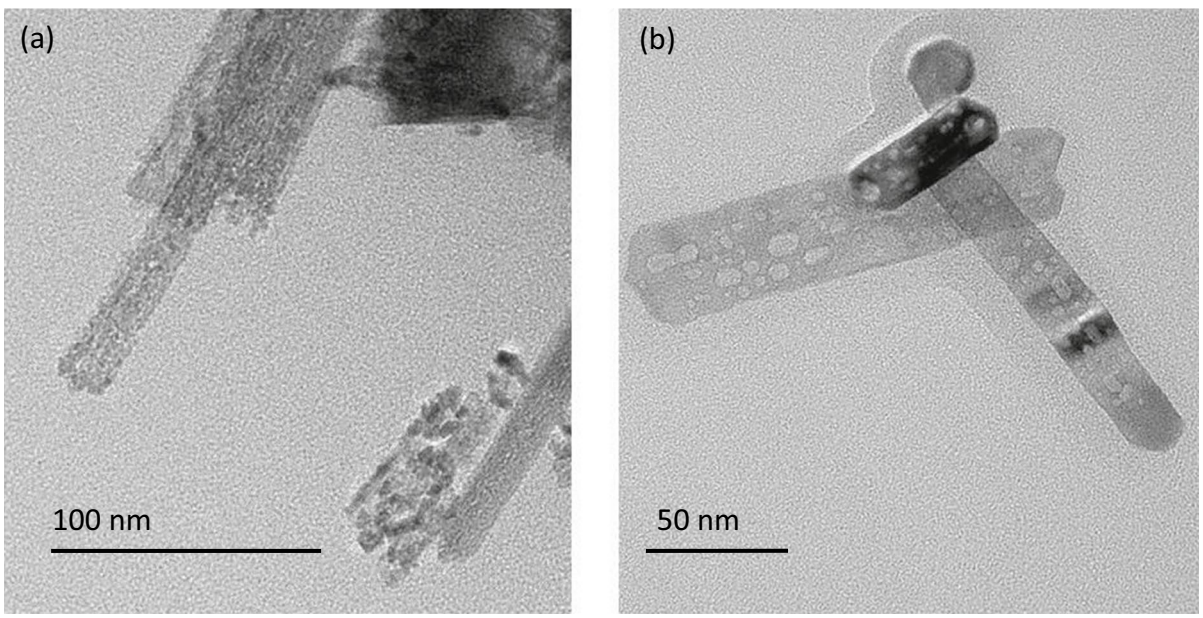

Fig. 1 Overview of a typical ceria nanorod sample before (**a**) and after (**b**) heat treatment to 800 °C; (modified from [23]). The wide rod of **b** shows multiple rows of voids across the entire rod volume and is a type 1 rod with < 110 > rod axis, enclosed by {100}/{110} facets

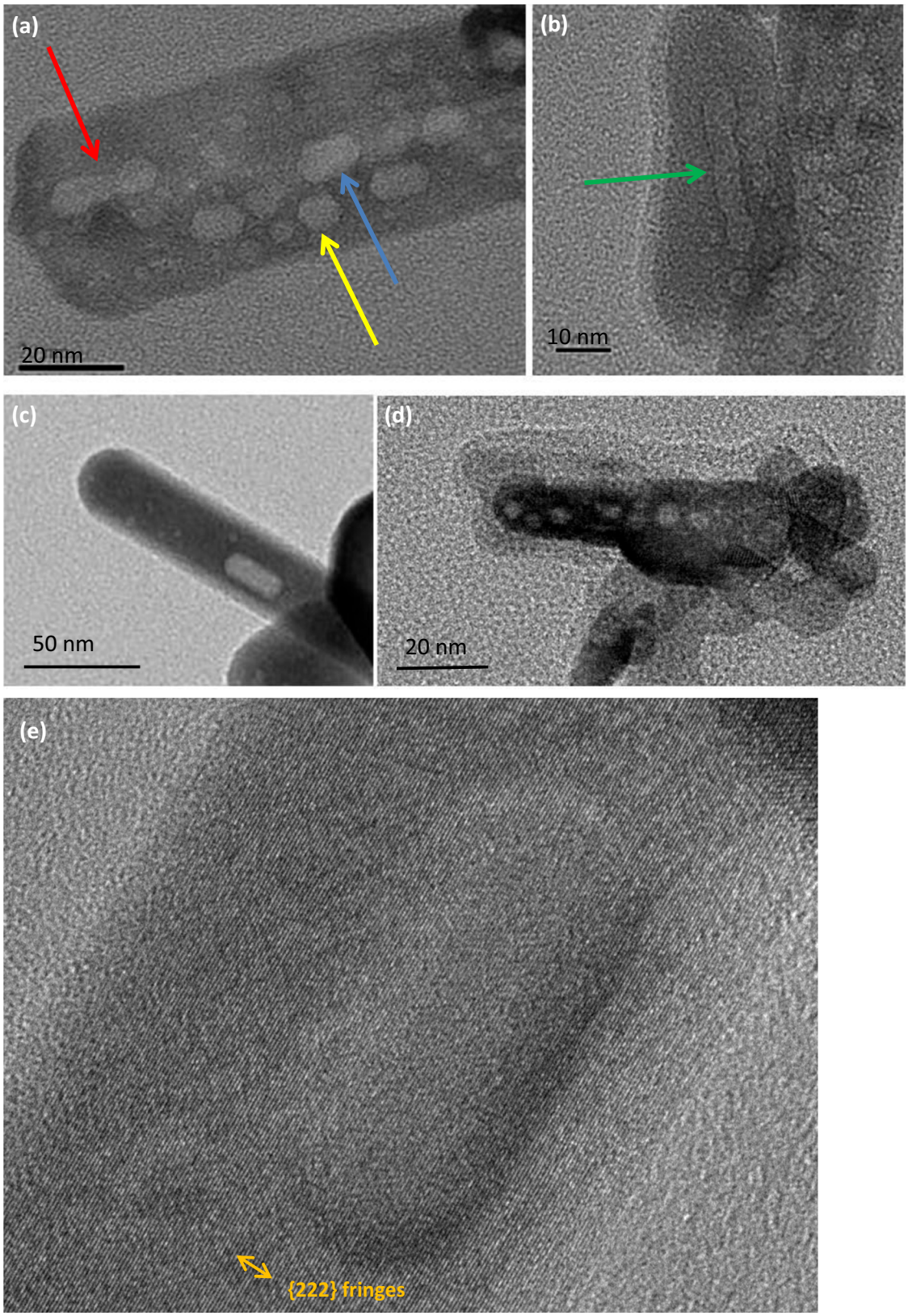
(a)
20 nm
(b)
10 nm
(c)
50 nm
(d)
20 nm
(e)
{222} fringes

◂**Fig. 2** Ceria nanorods heated at 800 °C (**a**, **b**, **d**) or at 950 °C (**c**, **e**) showing void space oriented attachment of cuboctahedral voids into voids of more tubular style. **a** Magnified section from Fig. 1b: standard void (yellow arrow), elongated void (blue arrow: typical example), and one case of a pair of voids in the process of merging (red arrow); (modified from [23]). **b** Longer void with non-straight surfaces (green arrow) indicating an origin from pre-existing negative particle shaped voids. **c** Elongated void at higher temperature with the void matching the external rod in both orientation and straightness of faces. **d** Chain of voids central to nanorod. In this case, all individual voids remain isotropic and near equidistant. **e** HRTEM of image **c** to show lattice fringe parallelity between pore surface and rod surface, with 10 fringes of 1.58 nm total indicated for scale

In order to achieve a transformation from octahedron building blocks to a 1D-nanorod external shape, the facet distribution needs to adapt, as the truncated octahedra show mainly {111} with small {100} caps. After oriented attachment using truncated octahedral CNPs, a growth into rods can be achieved in two ways [12]. Type 1 ceria nanorods (CNRs) develop new {110} surfaces, and new massively enlarged {100} faces, while the occurrence of {111} vanishes. Type 2 CNRs on the other hand maintain {111} type surfaces but swap the {100} of CNPs against {110} type rod faces. A third possible mechanism in which CNPs align into chains of {100} connected octahedra with <001> rod direction does not lead to flat CNRs and is not observed in this research. For details of the two types of rods that occurred, including their crystallography from lattice fringes and diffraction peaks, see [12, 22, 24].

After heat treatment, wider rods, such as in Fig. 1b, often have multiple parallel rows of voids, with the voids reaching over a quarter of the projected area within the solid rod. The distribution of voids is not random; rather, they often form chains of voids. Voids in chains do mostly not touch and they always stay clear of the rod surface, as we have already elucidated in our earlier tomography study [23]. This alignment is an important precursor to the possible next stages of formation of elongated rods, proposed below.

Void space oriented attachment

Various void systems inside multiple nanorods, even on the same sample, point to some diversity of microstructure. These differences are due to snapshots of rod morphology evolution recorded at different stages. Our evidence from multiple HRTEM micrographs is collected in Fig. 2, where isotropic voids (Fig. 2a, yellow arrow), as discussed in our previous work [23], and elongated voids coexist. This evidence points to the 1D growth of voids progressing in three stages:

(i) Fig. 2a shows predominantly a first stage, the initiation of void elongation upon heating to 800 °C. Aspect ratios are between 1.5:1 and 2:1, and the example with a blue arrow in Fig. 2a corresponds to 1.9:1.

(ii) Fig. 2b (also discovered on a particle heated to 800 °C) is an example where a second stage has developed via void-merging. The green-arrowed long void has its aspect ratio progressed to 6:1. However, the surfaces of the 6:1 void are not yet straight, and the initial size of individual octahedral void building blocks can be seen through the uneven diameter, especially when compared to single voids in the immediate vicinity. Also, the example of the red-arrowed double-void in Fig. 2a can be classified as early-stage 2 in this sense. The zig-zag surface of the green-arrowed void provides evidence that long voids do not grow by swallowing point defect vacancies but via merging of pre-existing voids.

Figure 2c shows a 3:1 aspect ratio void; however, this image is taken from a 950 °C heating sample. We propose this sample has undergone the third stage of transformation. Here, the void surfaces (as well as the rod surfaces) are perfectly smooth, and we conclude that via atomic diffusion, the zig-zagging rough surface of a stage-2 void has finally adopted an energetically more favourable shape with straight surfaces using the same surface energetics for the internal (void) and external (rod) surfaces. Figure 2d shows lattice fringes of void and rod surface oriented parallel to each other. The equivalence of rod surface and void surface even extends to a compatible radius of curvature for the rounded ends of the rod and the void. The orientation with {111} type surface, although seen here as half-period HRTEM fringes of (222) designation, corresponds to a "type 2" rod with <211> axis.

To remind of the diversity of rod morphologies observed on any single TEM sample, Fig. 2d shows a

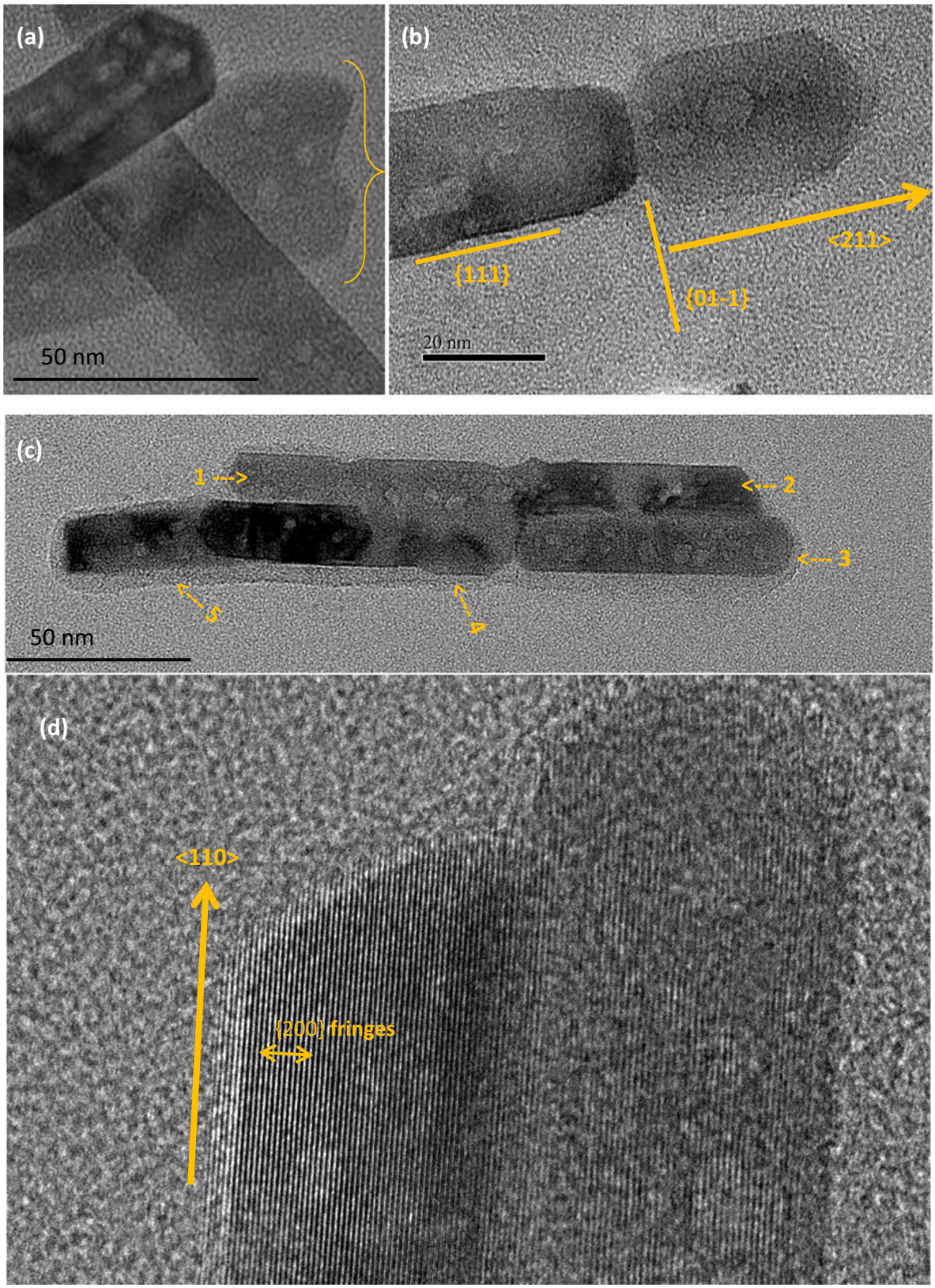
(a)
50 nm
(b)
{111}
<211>
{01-1}
20 nm
(c)
1 -->
<-- 2
<-- 3
50 nm
(d)
<110>
{200} fringes

◂**Fig. 3** Oriented merging of multiple nanorods towards larger single crystalline rods. **a** Double-ended rod (orange bracket); (modified from [24]). **b** Rod-on-rod axial merger. **c** 4-rod merger with sub-rod annotations 1–5 used in the text. **d** HRTEM showing single crystalline lattice orientation relationship across the merged rods, with 10 fringes of 2.62 nm total indicated for scale

finding (at 800 °C) in which individual voids remain isotropic and spaced roughly equally from each other. This might indicate a barrier against void diffusion and merging and a delay in the negative rod-shaped void formation until such a time–temperature regime where it becomes unavoidable.

Rod-to-rod oriented attachment (secondary OA)

Here, we report multiple findings of larger ceria nanorods appearing to have formed from smaller pre-existing rods. The samples used in this part are the same as for the void space oriented attachment (section B); therefore, the rod attachment is simultaneous to 1D-void formation.

A double-ended rod is shown in Fig. 3a, heated to 800 °C. There are two mechanisms that could underlie the formation of such double-headed rods. In mechanism 1, the rod grows as a single rod with full diameter, but to avoid a high energy flat end it reconstructs into a facetted double head, with lower energy facets overcompensating for the growth in total surface area. In mechanism 2, the rod can form initially via the merging of 2 separate rods of similar diameter, each single-ended with energetically favoured end facets. Subsequently, oriented attachment along the longest surface (side of the rod) leads to a final merging of the initially loosely attracted rods into the chemically bonded rod with bonds indistinguishable from internal bonds. This approach is equivalent to what would be oriented attachment growth from octahedral particles into single rods during primary hydrothermal growth [12].

Further imaging is presented aiming to clarify the two speculated mechanisms. Figure 3b captures an epitaxial perfect merger of two-rod building blocks with the smaller particle on the right still preserving its original end facets. The neck zone of this type 1 rod is therefore restricted to [1–10] contact, perpendicular to the rod axis. Figure 3b, therefore, supports the second mechanism, while being incompatible with mechanism 1. This is a unique rod-specific attachment mechanism, as nanoparticles would not exhibit this {110} type contact zone. Finally, Fig. 3c shows a merger of 4 rods (it is believed that a 5th rod sits on top of the rod at the bottom left). The gap between sub-rods 1 and 4 indicates van der Waals attraction only; however, the right half of the contact zone of rods 1 and 4 has already developed an atomically sharp chemical bond. The longitudinal contact between rods 3 and 4 in Fig. 3c is an axial attachment (as is the case of Fig. 3b), however not yet recrystallized and retaining its round shape.

Figure 3d is a rotated zoom image of the right quarter of Fig. 3c: Its HRTEM resolved lattice fringes are shown to confirm the lattice merging of the originally two rods into one single crystal. Here, the rod orientation with surfaces and HRTEM fringes corresponding to the {200} system points to a "type 1" rod with <110> axis.

Some TEM samples have been found to contain a rather diverse distribution of nanorods, even if all individual rods should have formally experienced identical heat treatment. Figure 4 shows examples that seem to have less well progressed towards rod-to-rod oriented attachment despite reaching high temperatures (800 °C in 4a and 950 °C in 4b).

Near the top (large yellow box) of Fig. 4a are 3 rods closing in on a merger by lateral attachment but still with gaps and slight orientation mismatch. The smaller bottom yellow window shows the contrasting case of axial attachment, reaching an already atomically sharp bond, equivalent to Fig. 3b. Figure 4b is another case of incomplete or "failed" attachment: even at 950 °C, the rods do not touch, possibly due to blocking debris, but sintering starts to fill the gap with diffused material (yellow window top left).

At this point, it is important to separate artefact carbon contamination from true sample material. During the extended TEM session electron, beam-induced deposition from residual hydrocarbon molecules results in all ceria nanorods being encased in an amorphous carbon layer. The thickness varies with exposure time and focusing of beam intensity. This is particularly visible in Figs. 1b, 2b, 2d, 3c, and 4a. As the layer grows after finishing sample heat treatment, it does not influence our observations and conclusions. Where the carbon appears to fill the space between neighbouring rods, e.g. Figure 4a, we should assume empty space at the start of the TEM session.

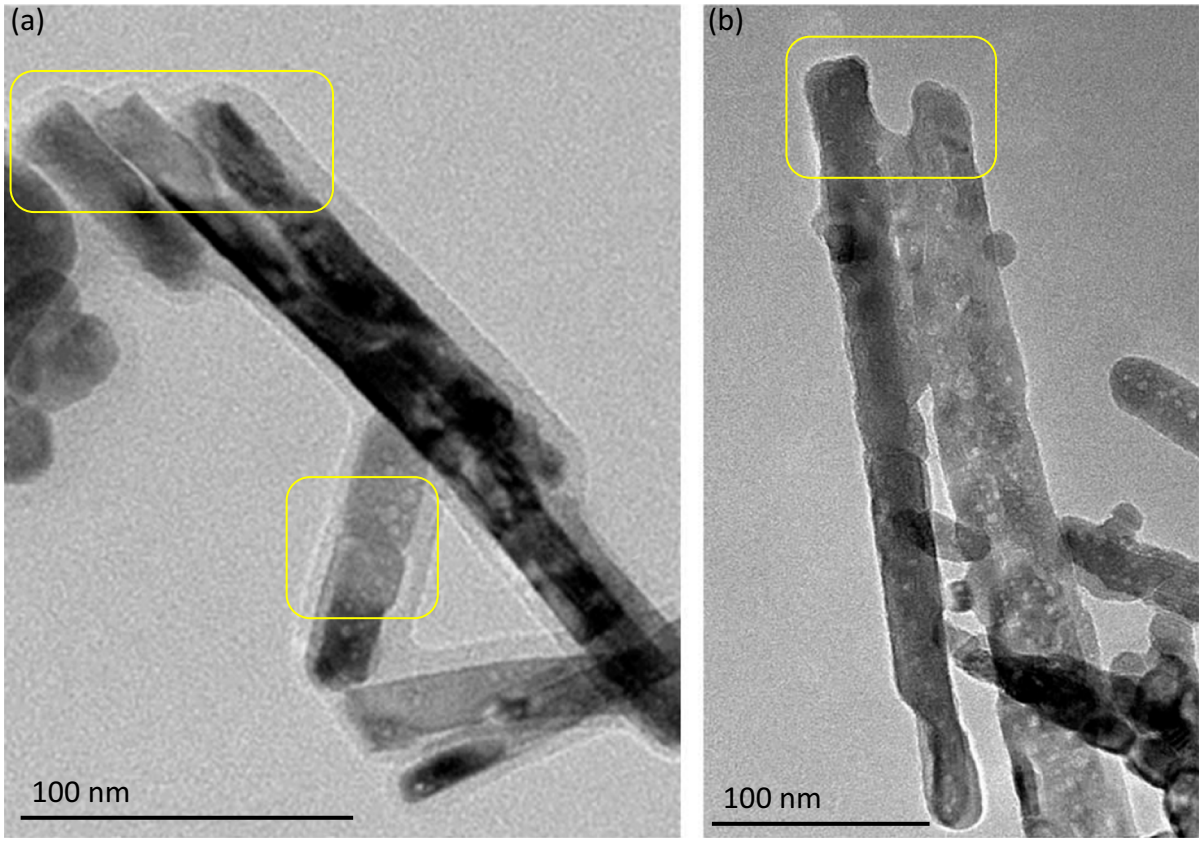

Fig. 4 Imperfect or incomplete rod merger. **a** A rod assembly after 800 °C heating, with the large and small boxes indicating regions discussed in the text. **b** From a 950 °C-heated sample, with the top end being discussed

The occurrence of perfect and imperfect cases of rod attachment on the same specimen indicates some kinetic delays, a dependency on random initial relative positions, and likely some dependence on mutual orientations. There could also be a small influence on the position of a rod within the larger powder during furnace heating.

The final observation is about rods that are close to forming a nanotube with the continuous cylindrical axial void. Figure 5 is a sample showing at least four elongated void spaces, distributed over 3 rods (orange arrows). Two examples are negative rod-shaped pores considered internally merged pores (voids 2 and 3 of Fig. 5 to compare with Fig. 2b). Also, we see a pair of voids (void 4), at the earliest stage of merging, with the top half retaining a cuboctahedral shape initially. Other void spaces (red arrows) are seemingly a residual from a gap during attachment with no re-orientation achieved, or alternatively, possibly broken attachment during preparation.

Discussion

In our previous work [23], we described "isotropic" voids in ceria nanorods of predominantly cuboctahedral shape, underpinned by molecular modelling calculations confirming these voids as favourable through energy minimisation. The multiple stages of hydrothermal growth and post-growth heat treatment applied to the nanorod samples, however, allow for kinetic considerations to play equally important roles. Also, the positions of the void with respect to rod surfaces and the rod geometry itself contribute to a greater diversity of void shapes reported in our new work here. Primarily, we now report elongated voids, of a "negative

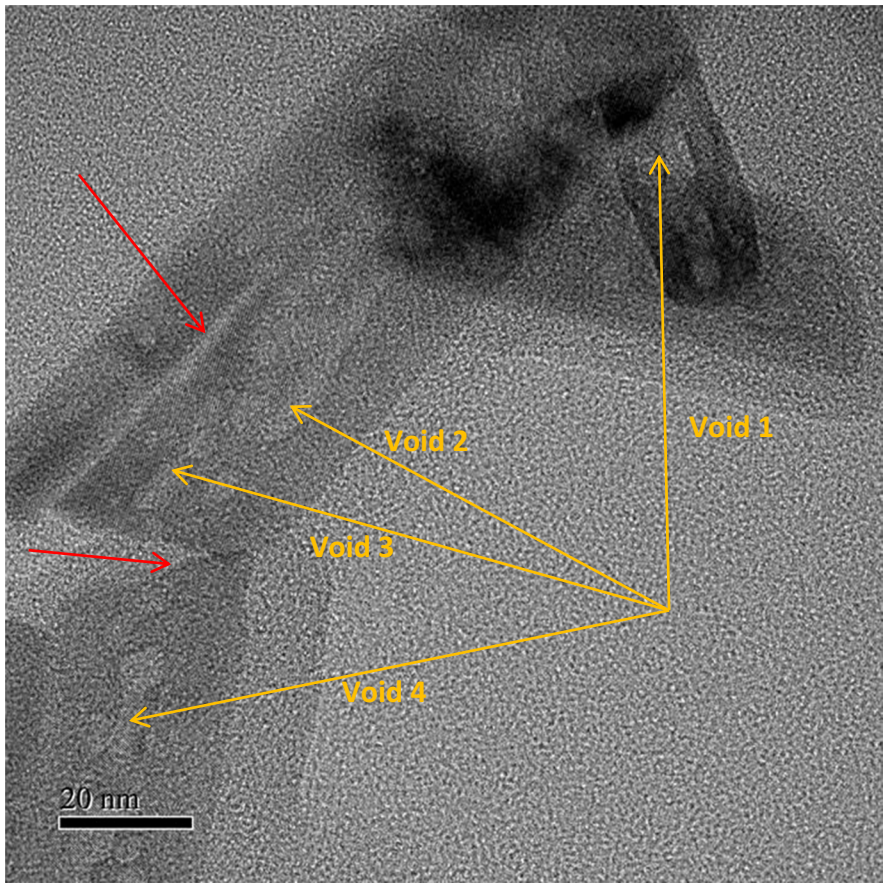

Fig. 5 Nanorods showing the transition to tubular structure (orange arrows). Further examples of incomplete attachment (red arrows)

rod" shape rather than a "negative-cuboctahedral" shape. The long axis of the elongated voids is always aligned with the rod axis, and they tend to prefer locations central to the rod. For geometrical reasons, there would not be a one-step linear and straight growth mechanism of rods directly from octahedra, as the rods consist of {111} combined with {110} planes, while the voids are {111} with {100}. For solid nanoparticles, this has been resolved by the oriented attachment mechanisms involving zig-zag attachments of cuboctahedral particles into <211> (or <110>) axis rods (see Fig. 5 in [12]).

Chains of cuboctahedral nanoparticles turning into nanorods have also been examined by molecular modelling [13], with neighbouring particles initially touching on {100} or {111} and forming zig-zag chains. Further studies of pair-wise agglomeration and chain formation are reported by Kim et al. [40]. Such a zig-zag chain-like state, translated from particle to void space, would correspond halfway between Fig. 2d and b. While this has not been captured here directly, it may well be inferred.

As sketched in Fig. 6, the 1D voids would form in the first step (6a to 6b) via aggregation of neighbouring voids to minimise further total surface energy, turning into a zig-zag elongated void as the intermediate stage. This is followed (6b to 6c) by further transformation during a long enough holding time of the heat treatment flattening surfaces into smooth negative rods. Figure 6 uses simplified hexagons (grey colour) to illustrate building blocks of ceria nanorods, enclosed by {111} and {100} surfaces, while simplified void spaces are shaded. The final void in Fig. 6c would become enclosed by either {100/110} or {111/110} depending on the rod axis being <110> or <211>. Blue interfaces drawn in Fig. 6 between neighbouring CNPs are an interim feature, as they no longer exist after successful completion of primary OA.

It appears straightforward to extrapolate that in a possible following stage via further (longer holding

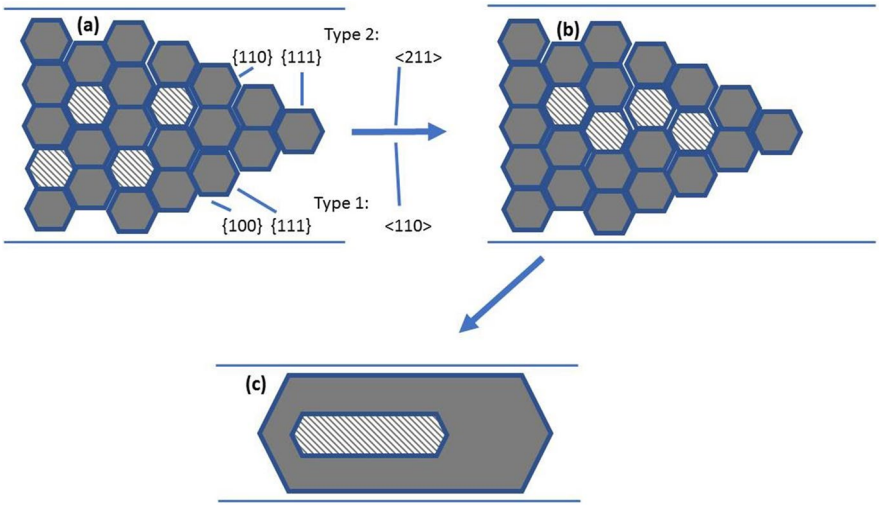

Fig. 6 Schematic formation of elongated voids along nanorod axes. **a** to **b** Via void merger equivalent to the nanoparticulate oriented attachment. **b** to **c** Via surface reconstruction and straightening of voids. The indexing examples are for a type 1 and type 2 nanorod. Schematic drawing only, not to scale

time) heat treatment and growth or merger of these rod-shaped voids, we finally end up forming ceria nanotubes, like those reported in [34–36]. Such fully formed nanotubes have not been observed in our study here, and they would be restricted to cases where enough voids exist to transform the rod into a symmetric tube. In the case of wider rods (Fig. 1; Fig. 2a) with multiple rows of voids, this would certainly be the case.

For the second main finding of rod-to-rod attachment, it is proposed that the main effect is already inherent during the hydrothermal growth stage. This might itself break down into initial loose alignment or aggregation of multiple rods into bundles followed by a closer contact and formation of interfaces and grain boundaries, although with defects. During the secondary dry heating under air, the rod attachment does not develop further in itself, at least not up to including 800 °C. However, as we know that this heat treatment mobilises defects and reconstructs surfaces and void morphologies [23], it is likely that the elimination of defects assists the conversion of past rod surfaces or grain boundaries into the perfect internal lattice, indistinguishable from rod centre areas (i.e. grain boundary-free). From above 950 °C, the onset of external materials flows, and then allows additional mechanisms, such as the filling of gaps between rods, or the rounding of corners, which leads to further smoothening and preferential formation of larger aggregates, eventually turning into sintered particles. The latter would also include Ostwald ripening if particles of more different sizes were available. However, unlike in the comparison by Lin et al. [41], oriented attachment and possible Ostwald ripening/sintering are seen here as strictly sequential, not as parallel alternatives. Another difference, referring to results part B, is that our mesopores do not form during but exclusively after hydrothermal growth as part of dry annealing. Therefore, gaps between touching nanoparticles during primary—imperfect—OA are also not seen as a major reason for pore formation.

We finally point to our new technique used for Fig. 4, which postponed annealing for up to 800 °C or 950 °C in a dry air furnace until after the nanopowders were dispersed on a TEM-transparent Si/Si_3N_4 membrane. This confirms the extraordinary thermal and chemical robustness of these thin membranes and opens new possibilities in studying thermal heat treatment of nanopowders with TEM imaging before and after heating, thus avoiding the heating under vacuum that would normally apply for in situ TEM heating holders, as shown in [22], and is atypical to simulate standard environmental laboratory heating processes.

Conclusions

Oriented attachment (OA) is presented as a mechanism of crystal morphology growth which, as a concept, appears more widely applicable than just in its original guise as a nanoparticle into nanorod transformation. We report evidence of voids in crystals aggregating and merging under secondary dry heat treatment of originally hydrothermally grown ceria

nanorods. As the shape of the voids corresponds initially to "negative" well-facetted particles, the surface energetics are equivalent whether aggregating solid particles in vacuum or multiple voids inside a single crystalline solid. Our second result points to the occurrence of a secondary oriented attachment consisting of small nanorods merging into fewer bigger nanorods, where the small nanorods would have experienced a primary OA during hydrothermal growth already. Minimising surface energies is the driving force here as well.

Funding This work was in part supported by CONACYT, Ministry of Energy, Hydrocarbons, Mexico, under the declaration HYDROCARBONS–HUMAN RESOURCES 2013–01; Henry Royce Institute for Advanced Materials; EPSRC: EP/R00661X/1, EP/S019367/1, EP/P02470X/1, and EP/P025285/1; and JEOL F-200 access at Royce@Sheffield.

Declarations

Conflict of interest The authors declare no competing interests.

References

1. Sun C, Li H, Chen L (2012) Nanostructured ceria-based materials: synthesis, properties, and applications. Energy Environ Sci 5:8475–8505. https://doi.org/10.1039/c2ee22310d
2. Seal S, Jeyaranjan A, Neal CJ et al (2020) Engineered defects in cerium oxides: tuning chemical reactivity for biomedical, environmental, & energy applications. Nanoscale 12:6879–6899. https://doi.org/10.1039/D0NR01203C
3. Gangopadhyay S, Frolov DD, Masunov AE, Seal S (2014) Structure and properties of cerium oxides in bulk and nanoparticulate forms. J Alloy Compd 584:199–208. https://doi.org/10.1016/j.jallcom.2013.09.013
4. Trovarelli A, Llorca J (2017) Ceria catalysts at nanoscale: how do crystal shapes shape catalysis? ACS Catal 7:4716–4735. https://doi.org/10.1021/acscatal.7b01246
5. Mullins DR (2015) The surface chemistry of cerium oxide. Surf Sci Rep 70:42–85. https://doi.org/10.1016/j.surfrep.2014.12.001
6. Sayle TXT, Caddeo F, Zhang X et al (2016) Structure–activity map of ceria nanoparticles, nanocubes, and mesoporous architectures. Chem Mater 28:7287–7295. https://doi.org/10.1021/acs.chemmater.6b02536
7. Aneggi E, Wiater D, de Leitenburg C et al (2014) Shape-dependent activity of ceria in soot combustion. ACS Catal 4:172–181. https://doi.org/10.1021/cs400850r
8. Castanet U, Feral-Martin C, Demourgues A et al (2019) Controlling the 111}/{110 surface ratio of cuboidal ceria nanoparticles. ACS Appl Mater Interfaces 11:11384–11390. https://doi.org/10.1021/acsami.8b21667
9. Sayle TXT, Molinari M, Das S et al (2013) Environment-mediated structure, surface redox activity and reactivity of ceria nanoparticles. Nanoscale 5:6063. https://doi.org/10.1039/c3nr00917c
10. Bhatta UM, Reid D, Sakthivel T et al (2013) Morphology and surface analysis of pure and doped cuboidal ceria nanoparticles. The Journal of Physical Chemistry C 117:24561–24569. https://doi.org/10.1021/jp405993v
11. Zhang D, Du X, Shi L, Gao R (2012) Shape-controlled synthesis and catalytic application of ceria nanomaterials. Dalton Trans 41:14455–14475. https://doi.org/10.1039/c2dt31759a
12. Du N, Zhang H, Chen B et al (2007) Ligand-free self-assembly of ceria nanocrystals into nanorods by oriented attachment at low temperature. The Journal of Physical Chemistry C 111:12677–12680. https://doi.org/10.1021/jp074011r
13. Sayle TXT, Inkson BJ, Karakoti A et al (2011) Mechanical properties of ceria nanorods and nanochains; the effect of dislocations, grain-boundaries and oriented attachment. Nanoscale 3:1823. https://doi.org/10.1039/c0nr00980f
14. Sayle TXT, Cantoni M, Bhatta UM et al (2012) Strain and architecture-tuned reactivity in ceria nanostructures; enhanced catalytic oxidation of CO to CO2. Chem Mater 24:1811–1821. https://doi.org/10.1021/cm3003436
15. Sakthivel T, Das S, Kumar A et al (2013) Morphological phase diagram of biocatalytically active ceria nanostructures as a function of processing variables and their properties. ChemPlusChem 78:1446–1455. https://doi.org/10.1002/cplu.201300302
16. Xu Y, Mofarah SS, Mehmood R et al (2021) Design strategies for ceria nanomaterials: untangling key mechanistic concepts. Mater Horiz 8:102–123. https://doi.org/10.1039/D0MH00654H
17. Symington AR, Harker RM, Storr MT et al (2020) Thermodynamic evolution of cerium oxide nanoparticle morphology using carbon dioxide. The Journal of Physical Chemistry C 124:23210–23220. https://doi.org/10.1021/acs.jpcc.0c07437
18. Symington AR, Molinari M, Moxon S et al (2020) Strongly bound surface water affects the shape evolution of cerium oxide nanoparticles. The Journal of Physical Chemistry C 124:3577–3588. https://doi.org/10.1021/acs.jpcc.9b09046

19. Minervini L (1999) Defect cluster formation in M2O3-doped CeO2. Solid State Ionics 116:339–349. https://doi.org/10.1016/S0167-2738(98)00359-2
20. Liu X, Zhou K, Wang L et al (2009) Oxygen vacancy clusters promoting reducibility and activity of ceria nanorods. J Am Chem Soc 131:3140–3141. https://doi.org/10.1021/ja808433d
21. Florea I, Feral-Martin C, Majimel J et al (2013) Three-dimensional tomographic analyses of CeO $_2$ nanoparticles. Cryst Growth Des 13:1110–1121. https://doi.org/10.1021/cg301445h
22. Sakthivel TS, Reid DL, Bhatta UM et al (2015) Engineering of nanoscale defect patterns in CeO2 nanorods via ex situ and in situ annealing. Nanoscale 7:5169–5177. https://doi.org/10.1039/C4NR07308H
23. Brambila C, Sayle DC, Molinari M et al (2021) Tomographic study of mesopore formation in ceria nanorods. The Journal of Physical Chemistry C 125:10077–10089. https://doi.org/10.1021/acs.jpcc.1c01221
24. Zhang S, Chang C-R, Huang Z-Q et al (2016) High catalytic activity and chemoselectivity of sub-nanometric Pd clusters on porous nanorods of CeO 2 for hydrogenation of nitroarenes. J Am Chem Soc 138:2629–2637. https://doi.org/10.1021/jacs.5b11413
25. Castell MR (2003) Wulff shape of microscopic voids in UO2 crystals. Phys Rev 68:235411. https://doi.org/10.1103/PhysRevB.68.235411
26. Han WQ, Wu L, Klie RF, Zhu Y (2007) Enhanced optical absorption induced by dense nanocavities inside titania nanorods. Adv Mater 19:2525–2529. https://doi.org/10.1002/adma.200700540
27. Penn RL, Banfield JF (1999) Morphology development and crystal growth in nanocrystalline aggregates under hydrothermal conditions: insights from titania. Geochim Cosmochim Acta 63:1549–1557. https://doi.org/10.1016/S0016-7037(99)00037-X
28. Penn RL (1979) Banfield JF (1998) Imperfect oriented attachment: dislocation generation in defect-free nanocrystals. Science 281:969–971. https://doi.org/10.1126/science.281.5379.969
29. De Yoreo JJ, Gilbert PUPA, Sommerdijk NAJM et al (2015) Crystallization by particle attachment in synthetic, biogenic, and geologic environments. Science 349(6247):aaa6760. https://doi.org/10.1126/science.aaa6760
30. Bahrig L, Hickey SG, Eychmüller A (2014) Mesocrystalline materials and the involvement of oriented attachment – a review. CrystEngComm 16:9408–9424. https://doi.org/10.1039/C4CE00882K
31. Godinho M, Ribeiro C, Longo E, Leite ER (2008) Influence of microwave heating on the growth of gadolinium-doped cerium oxide nanorods. Cryst Growth Des 8:384–386. https://doi.org/10.1021/cg700872b
32. Zhang H, de Yoreo JJ, Banfield JF (2014) A unified description of attachment-based crystal growth. ACS Nano 8:6526–6530. https://doi.org/10.1021/nn503145w
33. Thomele D, Baumann SO, Schneider J et al (2021) Cubes to cubes: organization of MgO particles into one-dimensional and two-dimensional nanostructures. Cryst Growth Des 21:4674–4682. https://doi.org/10.1021/acs.cgd.1c00535
34. Zhang R, Lu K, Zong L et al (2017) Gold supported on ceria nanotubes for CO oxidation. Appl Surf Sci 416:183–190. https://doi.org/10.1016/j.apsusc.2017.04.158
35. Tang Z-R, Zhang Y, Xu YJ (2011) A facile and high-yield approach to synthesize one-dimensional CeO2 nanotubes with well-shaped hollow interior as a photocatalyst for degradation of toxic pollutants. RSC Adv 1:1772–1777. https://doi.org/10.1039/c1ra00518a
36. Wang Z, Yu R (2019) Hollow micro/nanostructured ceria-based materials: synthetic strategies and versatile applications. Adv Mater 31:1800592. https://doi.org/10.1002/adma.201800592
37. Martin P, Parker SC, Sayle DC, Watson GW (2007) Atomistic modeling of multilayered ceria nanotubes. Nano Lett 7:543–546. https://doi.org/10.1021/nl0626737
38. Stelmachowski P, Ciura K, Indyka P, Kotarba A (2017) Facile synthesis of ordered CeO 2 nanorod assemblies: morphology and reactivity. Mater Chem Phys 201:139–146. https://doi.org/10.1016/j.matchemphys.2017.08.038
39. Chen DJ, Wang YJ, Wei K et al (2007) Self-organization of hydroxyapatite nanorods through oriented attachment. Biomaterials 28:2275–2280. https://doi.org/10.1016/j.biomaterials.2007.01.033
40. Kim B-H, Kullgren J, Wolf MJ et al (2019) Multiscale modeling of agglomerated ceria nanoparticles: interface stability and oxygen vacancy formation. Front Chem 7:203. https://doi.org/10.3389/fchem.2019.00203
41. Lin M, Fu ZY, Tan HR et al (2012) Hydrothermal synthesis of CeO2 nanocrystals: Ostwald ripening or oriented attachment? Cryst Growth Des 12:3296–3303. https://doi.org/10.1021/cg300421x